

February 8, 2020
hep-ph/01xxx

Complete next-to-leading order QCD corrections to charged Higgs boson associated production with top quark at the CERN Large Hadron Collider

SHOU-HUA ZHU

*Institut für Theoretische Physik, Universität Karlsruhe,
D-76128 Karlsruhe, Germany*

The complete next-to-leading order (NLO) QCD corrections to charged Higgs boson associated production with top quark through $bg \rightarrow tH^-$ at the CERN Large Hadron Collider are calculated in the minimal supersymmetric standard model (MSSM) and two-Higgs-doublet model in the \overline{MS} scheme. The NLO QCD corrections can reduce the scale dependence of the leading order (LO) cross section. The K-factor (defined as the ratio of the NLO cross section to the LO one) varies roughly from ~ 1.6 to ~ 1.8 when charged Higgs mass increases from 200 GeV to 1000 GeV.

I. INTRODUCTION

The detection of the Higgs particles is one of the most important objectives of the Large Hadron Collider (LHC). Charged Higgs boson are predicted in extended versions of the Standard model (SM), like two-Higgs-doublet models (2HDM) and the Minimal Supersymmetric Standard Model (MSSM). Discovery of such an additional charged Higgs boson will immediately indicate physics beyond the SM, unlike the case of the neutral Higgs boson. Hence, there is strong theoretical and experimental motivation for exploring the mechanisms of the charged Higgs boson production.

The charged Higgs boson H^\pm could appear as the decay product of primarily produced top quarks if the mass of H^\pm is smaller than $m_t - m_b$. For heavier H^\pm , the direct H^\pm production mechanisms at hadron colliders have been extensively investigated. At the LHC, the primary charged Higgs boson production channel is $gb \rightarrow H^- t$ [1] *. The study [3,4] shows that this production mechanism can be used to explore the parameter space of MSSM for m_{H^\pm} up to 1 TeV and $\tan\beta$ down to at least ~ 3 , and potentially to ~ 1.5 . Therefore, it is necessary to calculate and implement also the loop contributions to $gb \rightarrow H^- t$ for more accurate theoretical predictions.

In literature, the contribution of the initial-gluon process $gg \rightarrow H^- t \bar{b}$, which is only part of the next-to-leading order (NLO) QCD corrections to $gb \rightarrow H^- t$, has been calculated [5]. The supersymmetric electroweak corrections arising from the quantum effects which are induced by potentially large Yukawa couplings from the Higgs sector and the chargino-top(bottom)-sbottom(stop) couplings, neutralino- top(bottom)-stop(sbottom) couplings and charged Higgs-stop-sbottom couplings are also studied [1,6], which can give rise to a 15% reduction of the lowest-order result. In Ref. [7], the electro-weak corrections to the process are also discussed. Recently, the study on the SUSY-QCD effect for this process is also done [8]. In this paper, we deal with the complete NLO QCD corrections to $gb \rightarrow H^- t$, which is much complicated calculations than what has been done, and that is part of the reason why the calculation is not available until now.

* See Ref. [2] for the discussion on other charged Higgs boson production mechanisms.

The arrangement of this paper is as follows. Section II contains the analytic results, and in Section III we present numerical examples and discuss the implications of our results. The lengthy expressions of the form factors are collected in the Appendix.

II. ANALYTIC EXPRESSIONS

Including the NLO QCD corrections, the cross sections for $PP \rightarrow tH^-X$ at the CERN LHC can be written as

$$\sigma = \sigma^{LO} + \sigma^{Vir} + \sigma^{Real}, \quad (1)$$

where σ^{LO} is the cross section at leading order (LO), σ^{Vir} and σ^{Real} are cross sections from NLO QCD corrections arising from virtual and real processes.

A. LO cross section

The Feynman diagrams for the charged Higgs boson production via $b(p_1)g(p_2) \rightarrow t(k_1)H^-(k_2)$ at the LO are shown in Fig.1. The amplitudes are created by use of Feynarts [9] and are handled with the help of FeynCalc [10]. As usual, we define the Mandelstam variables as

$$\begin{aligned} s &= (p_1 + p_2)^2 = (k_1 + k_2)^2, \\ t &= (p_1 - k_1)^2 = (p_2 - k_2)^2, \\ u &= (p_1 - k_2)^2 = (p_2 - k_1)^2. \end{aligned} \quad (2)$$

The amplitude at the LO could be written as

$$M_{LO} = \sum_{i=1}^6 t_i [c_1 M_{2i-1} + c_2 M_{2i}], \quad (3)$$

where the non-vanishing form factors are

$$\begin{aligned} t_2 &= \frac{1}{m_t^2 - u} - \frac{1}{s}, \\ t_3 &= \frac{2}{m_t^2 - u}, \\ t_5 &= -\frac{2}{s}, \end{aligned} \quad (4)$$

where $c_1 = \frac{g_w g_s \mu^{2\epsilon} m_b \tan \beta}{2\sqrt{2} m_w}$ and $c_2 = \frac{g_w g_s \mu^{2\epsilon} m_t \cot \beta}{2\sqrt{2} m_w}$. In Eq. (3) M_i is the standard matrix elements which are defined as

$$\begin{aligned}
M_1 &= \bar{u}(k_1) \not{e}(p_2) P_R u(p_1), \\
M_2 &= \bar{u}(k_1) \not{e}(p_2) P_L u(p_1), \\
M_3 &= \bar{u}(k_1) \not{p}_2 \not{e}(k_2) P_R u(p_1), \\
M_4 &= \bar{u}(k_1) \not{p}_2 \not{e}(k_2) P_L u(p_1), \\
M_5 &= \bar{u}(k_1) P_R u(p_1) k_1 \cdot \varepsilon(p_2), \\
M_6 &= \bar{u}(k_1) P_L u(p_1) k_1 \cdot \varepsilon(p_2), \\
M_7 &= \bar{u}(k_1) \not{p}_2 P_R u(p_1) k_1 \cdot \varepsilon(p_2), \\
M_8 &= \bar{u}(k_1) \not{p}_2 P_L u(p_1) k_1 \cdot \varepsilon(p_2), \\
M_9 &= \bar{u}(k_1) P_R u(p_1) p_1 \cdot \varepsilon(p_2), \\
M_{10} &= \bar{u}(k_1) P_L u(p_1) p_1 \cdot \varepsilon(p_2), \\
M_{11} &= \bar{u}(k_1) \not{p}_2 P_R u(p_1) p_1 \cdot \varepsilon(p_2), \\
M_{12} &= \bar{u}(k_1) \not{p}_2 P_L u(p_1) p_1 \cdot \varepsilon(p_2), \tag{5}
\end{aligned}$$

where the color matrix T^a has been suppressed. In this paper, we perform the calculations in Feynman gauge and in d time-space dimensions with $d = 4 - 2\epsilon$. For simplicity, throughout the paper we omit the bottom quark dynamical mass but keep the mass-term only in Yukawa couplings.

The LO cross section can then be written as

$$\frac{d\sigma_{LO}}{dx_1 dx_2} = d\hat{\sigma}^0 G_{b/A}(x_1, \mu_f) G_{g/B}(x_2, \mu_f) + [A \leftrightarrow B], \tag{6}$$

with

$$d\hat{\sigma}^0 = \frac{1}{24} \frac{1}{4(1-\epsilon)} \frac{1}{2s} |M_{LO}|^2 d^N \Phi_2 \tag{7}$$

where the factor $\frac{1}{24}$ and $\frac{1}{4(1-\epsilon)}$ are the color and spin average, respectively, and two-body phase space is

$$d^N \Phi_2 = \frac{1}{8\pi} \left(\frac{4\pi}{s} \right)^\epsilon \frac{1}{\Gamma(1-\epsilon)} \left[\lambda \left(1, \frac{m_{H^\pm}^2}{s}, \frac{m_t^2}{s} \right) \right]^{1/2-\epsilon} v^{-\epsilon} (1-v)^{-\epsilon} dv, \tag{8}$$

with $v = \frac{1}{2}(1 + \cos \theta)$. Here λ is the two-body phase space function

$$\lambda(x, y, z) = x^2 + y^2 + z^2 - 2xy - 2xz - 2yz. \quad (9)$$

B. Virtual corrections

The Feynman diagrams for the NLO virtual corrections are shown in Fig. 2. The virtual diagrams which have the bubble on the external legs are not shown. They can be obtained by inserting diagram (a)-(d) of Fig. 2 into the external legs of the LO diagrams in Fig. 1. At the same time, the diagrams containing counter-terms can be easily got by inserting corresponding counter-terms into external legs, internal propagators and vertex of the LO diagrams.

In order to remove the UV divergences, we have to renormalize the strong coupling constant, the Yukawa coupling constants, the quark masses and the wave functions of quarks and gluon. The strong coupling constant and the gluon wave function are renormalized as

$$\begin{aligned} \frac{\delta g_s}{g_s} &= -\frac{\alpha_s}{8\pi} \beta_0 \Delta, \\ Z_g &= -\frac{\alpha_s}{4\pi} (2C_A - \beta_0) \Delta, \end{aligned} \quad (10)$$

with $\Delta = \frac{1}{\epsilon} - \gamma_E + \log(4\pi)$, $\beta_0 = (11C_A - 2n_f)/3$, $C_A = 3$ and $C_F = 4/3$.

For the renormalization of the bottom quark, we choose

$$\begin{aligned} \frac{\delta m_b}{m_b} &= -\frac{\alpha_s}{4\pi} 3C_F \Delta, \\ Z_b &= -\frac{\alpha_s}{4\pi} C_F \Delta, \end{aligned} \quad (11)$$

which makes terms like $\alpha_s \log(m_b^2/\mu^2)$ be resummed into the running of the b quark mass. In order to show that the renormalization of the b quark mass here is appropriate, we will renormalize the top quark mass in two schemes: on-mass-shell (OS) and \overline{MS} .

$$\begin{aligned} \frac{\delta m_t}{m_t} &= -\frac{\alpha_s}{4\pi} 3C_F \left[\Delta + \frac{4}{3} - \log(m_t^2/\mu^2) \right], \quad \text{in OS scheme} \\ \frac{\delta m_t}{m_t} &= -\frac{\alpha_s}{4\pi} 3C_F \Delta, \quad \text{in } \overline{MS} \text{ scheme.} \end{aligned} \quad (12)$$

Hereafter we will refer OS and \overline{MS} schemes to the different mass renormalization of the top quark. The comparison between the results in these two schemes will be discussed in the

numerical section. The wave function renormalization constant of top quark is chosen the same with that of b quark

$$Z_t = -\frac{\alpha_s}{4\pi} C_F \Delta. \quad (13)$$

The renormalized virtual amplitude can then be written in the following way,

$$M_{\text{ren}} = M_A + M_B, \quad (14)$$

where M_A is the amplitude from the diagram (e)-(o) of Fig. 2 and M_B is the amplitude from the diagrams which contain bubble on the external legs or counter-terms.

The M_A can be written as

$$M_A = \sum_{i=e}^o M_A^i, \quad (15)$$

where i represents the diagram index of Fig. 2. For each diagram i , we can generally write the amplitude as

$$M_A^i = \sum_{j=1}^6 f_j [c_1 M_{2i-1} + c_2 M_{2i}], \quad (16)$$

where the non-vanishing form factor f_j are given explicitly in Appendix and the M_j is the standard matrix element given in the previous subsection.

The M_B can be written as

$$M_B = M_B^1 + M_B^2, \quad (17)$$

where

$$M_B^1 = M_{LO} \left\{ \frac{\delta g_s}{g_s} + \frac{Z_t}{2} + \frac{Z_b}{2} + \frac{Z_g}{2} + \frac{\alpha_s}{8\pi} \left[-3\Delta + \frac{14}{3} \log(m_t^2/\mu^2) - \frac{16}{3} \right] \right\}, \quad (18)$$

$$M_B^2 = \sum_{i=1}^6 [c_1 f_s^{2i-1} M_{2i-1} + c_2 f_s^{2i} M_{2i}]. \quad (19)$$

Here the non-vanishing form factors f_s^i ($i = 1 - 12$) are

$$\begin{aligned} f_s^1 &= f_s^2 = \frac{\delta m_t}{m_t^2 - u}, \\ f_s^3 &= \frac{-2m_t \delta m_t}{(m_t^2 - u)^2} + \frac{\delta m_b}{m_b} \left[\frac{1}{m_t^2 - u} - \frac{1}{s} \right], \end{aligned}$$

$$\begin{aligned}
f_s^4 &= \frac{-2m_t\delta m_t}{(m_t^2 - u)^2} + \frac{\delta m_t}{m_t} \left[\frac{1}{m_t^2 - u} - \frac{1}{s} \right], \\
f_s^5 &= 2 \left[\frac{-2m_t\delta m_t}{(m_t^2 - u)^2} + \frac{\delta m_b}{m_b} \frac{1}{m_t^2 - u} \right], \\
f_s^6 &= 2 \left[\frac{-2m_t\delta m_t}{(m_t^2 - u)^2} + \frac{\delta m_t}{m_t} \frac{1}{m_t^2 - u} \right], \\
f_s^9 &= -\frac{2}{s} \frac{\delta m_b}{m_b}, \\
f_s^{10} &= -\frac{2}{s} \frac{\delta m_t}{m_t}.
\end{aligned} \tag{20}$$

After squaring the renormalized amplitude and performing the spin and color summations, the partonic cross section with virtual corrections can be written as

$$\frac{d\sigma^{Vir}}{dx_1 dx_2} = 2 \operatorname{Re} \left[\overline{\sum} (M_{\text{ren}}^+ M_{LO}) \right] d^N \Phi_2 G_{b/A}(x_1, \mu_f) G_{g/B}(x_2, \mu_f) + [A \leftrightarrow B]. \tag{21}$$

After the renormalization procedure described above, $d\sigma^{Vir}$ is UV-finite. Nevertheless, it contains still the infrared and collinear divergences. The infrared divergences will cancel against the contributions from real-gluon radiation [see Eq. (23)]. The remaining collinear divergences in the real-gluon-emission processes will be removed by the redefinition of the parton distribution functions (PDF) (mass factorization) [see Eq. (25)]. We have checked these kind of cancellations and won't give the explicit expressions here.

C. Real corrections

There are three kinds of real corrections to the processes $bg \rightarrow tH^-$: gluon-radiation [$bg \rightarrow tH^-g$], initial-gluon [$gg \rightarrow tH^-\bar{b}$] and initial-active-quark [$bq(\bar{q}) \rightarrow tH^-q(\bar{q})$ and $q\bar{q} \rightarrow tH^-\bar{b}$, where q stand for the active quarks which are treated as light for PDF evolution, in practice the light quarks other than u, d, s can be omitted due to the low luminosity]. All real corrections are related to the $2 \rightarrow 3$ processes.

In this paper, the $2 \rightarrow 3$ processes have been treated using the two cut-off phase space slicing method (TCPSSM) [12]. The method is briefly described in the following. Two small artificial constants δ_s, δ_c are introduced, and the three-body phase space can firstly be divided into soft and hard regions according to whether the gluon energy is less than $\delta_s \sqrt{s}/2$. Secondly the hard region is further divided into collinear and non-collinear regions according

to whether the magnitude of $p_i \cdot p_j$ is less than $s/2$. In the soft and collinear regions, the phase space integration can be performed analytically in d-dimension. At the same time, in the non-collinear region, the phase space integration can be calculated in four dimension by standard Monte Carlo packages because the integration contains no divergences. Obviously, the final physical results should be independent on these artificial parameters δ_s and δ_c , which offers a crucial way to check our results. Therefore, the real corrections can be written as, according to the phase space slicing,

$$d\sigma^{Real} = d\sigma^S + d\sigma^{Coll} + d\sigma^{fin}, \quad (22)$$

where $d\sigma^S$, $d\sigma^{Coll}$ and $d\sigma^{fin}$ are cross sections in soft, collinear and non-collinear regions.

1. Cross section in soft region

The Feynman diagrams of the gluon-radiation process $bg \rightarrow tH^-g$ are shown in Fig. 3. They are the only diagrams which contribute to the cross section in the soft region. We may write the cross section as

$$\begin{aligned} \frac{d\sigma^S}{dx_1 dx_2} &= d\hat{\sigma}_S^0 G_{b/A}(x_1, \mu_f) G_{g/B}(x_2, \mu_f) + [A \leftrightarrow B], \\ d\hat{\sigma}_S^0 &= d\hat{\sigma}^0 \left[\frac{\alpha_s}{2\pi} \frac{\Gamma(1-\epsilon)}{\Gamma(1-2\epsilon)} \left(\frac{4\pi\mu_r^2}{s} \right)^\epsilon \right] \left(\frac{A_2^s}{\epsilon^2} + \frac{A_1^s}{\epsilon} + A_0^s \right), \end{aligned} \quad (23)$$

where

$$\begin{aligned} A_2^s &= -\frac{4}{3} \frac{m_t^2 - t}{(E_1 - \beta \cos \theta)s} + 12 \frac{m_t^2 - u}{(E_1 + \beta \cos \theta)s} + 12, \\ A_1^s &= \frac{16}{3} \frac{4m_t^2}{(E_1^2 - \beta^2)s} + \frac{4}{3} \frac{m_t^2 - t}{(E_1 - \beta \cos \theta)s} (C_1 - 2 \log \frac{2}{\delta_s \sqrt{s}}) \\ &\quad + 12 \frac{m_t^2 - u}{(E_1 + \beta \cos \theta)s} (C_2 - 2 \log \frac{2}{\delta_s \sqrt{s}}) + 24 \log \frac{2}{\delta_s \sqrt{s}} - \log \frac{4}{s} A_2^s, \\ A_0^s &= \frac{1}{2} \log^2 \frac{4}{s} A_2^s - \log \frac{4}{s} A_1^s + \frac{16}{3} \frac{4m_t^2}{(E_1^2 - \beta^2)s} (2 \log \frac{2}{\delta_s \sqrt{s}} + \frac{E_1}{\beta} \log \frac{E_1 + \beta}{E_1 - \beta}) \\ &\quad + \frac{4}{3} \frac{m_t^2 - t}{(E_1 - \beta \cos \theta)s} (C_3 - 2 \log^2 \frac{2}{\delta_s \sqrt{s}} + 2C_1 \log \frac{2}{\delta_s \sqrt{s}}) \\ &\quad - 12 \frac{m_t^2 - u}{(E_1 + \beta \cos \theta)s} (C_4 - 2 \log^2 \frac{2}{\delta_s \sqrt{s}} + 2C_2 \log \frac{2}{\delta_s \sqrt{s}}) + 24 \log^2 \frac{2}{\delta_s \sqrt{s}}, \\ C_1 &= \log \frac{(E_1 - \beta \cos \theta)^2}{E_1^2 - \beta^2}, \end{aligned}$$

$$\begin{aligned}
C_2 &= \log \frac{(E_1 + \beta \cos \theta)^2}{E_1^2 - \beta^2}, \\
C_3 &= -\log^2 \frac{E_1 - \beta}{E_1 - \beta \cos \theta} + \frac{1}{2} \log^2 \frac{E_1 + \beta}{E_1 - \beta} - 2li_2\left(-\frac{-\beta \cos \theta + \beta}{E_1 - \beta}\right) + 2li_2\left(-\frac{\beta \cos \theta + \beta}{E_1 - \beta \cos \theta}\right), \\
C_4 &= -\log^2 \frac{E_1 - \beta}{E_1 + \beta \cos \theta} + \frac{1}{2} \log^2 \frac{E_1 + \beta}{E_1 - \beta} - 2li_2\left(-\frac{\beta \cos \theta + \beta}{E_1 - \beta}\right) + 2li_2\left(-\frac{-\beta \cos \theta + \beta}{E_1 + \beta \cos \theta}\right), \\
\beta &= \lambda^{\frac{1}{2}}(1, m_t^2/s, m_{H^\pm}^2/s), \\
E_1 &= \sqrt{\beta^2 + \frac{2m_t^2}{s}}.
\end{aligned} \tag{24}$$

2. Cross section in collinear region

In order to remove the collinear singularity, we should introduce a scale dependent parton distribution function (mass factorization). After factorization in $\overline{\text{MS}}$ convention, the cross section in collinear region can be written as

$$\begin{aligned}
\frac{d\sigma^{Coll}}{dx_1 dx_2} &= \left[\frac{\alpha_s}{2\pi} \frac{\Gamma(1-\epsilon)}{\Gamma(1-2\epsilon)} \left(\frac{4\pi\mu_r^2}{s} \right)^\epsilon \right] \left\{ G_{b/A}(x_1, \mu_f) G_{g/B}(x_2, \mu_f) \right. \\
&\quad \times \left[\frac{A_1^{sc}(b \rightarrow bg)}{\epsilon} + \frac{A_1^{sc}(g \rightarrow gg)}{\epsilon} + A_0^{sc}(b \rightarrow bg) + A_0^{sc}(g \rightarrow gg) \right] \\
&\quad \left. + G_{b/A}(x_1, \mu_f) \tilde{G}_{g/B}(x_2, \mu_f) + \tilde{G}_{b/A}(x_1, \mu_f) G_{g/B}(x_2, \mu_f) \right\} d\hat{\sigma}_0 \\
&\quad + [A \leftrightarrow B],
\end{aligned} \tag{25}$$

where [12]

$$A_0^{sc} = A_1^{sc} \ln \left(\frac{s}{u_f^2} \right) \tag{26}$$

$$A_1^{sc}(b \rightarrow bg) = C_F(2 \ln \delta_s + 3/2) \tag{27}$$

$$A_1^{sc}(g \rightarrow gg) = 2N \ln \delta_s + (11N - 2n_f)/6. \tag{28}$$

Here

$$\tilde{G}_{c/B,A}(x, \mu_f) = \sum_{c'} \int_x^{1-\delta_s \delta_{cc'}} \frac{dy}{y} G_{c'/B,A}(x/y, \mu_f) \tilde{P}_{cc'}(y) \tag{29}$$

with

$$\tilde{P}_{ij}(y) = P_{ij}(y) \ln \left(\delta_c \frac{1-y}{y} \frac{s}{\mu_f^2} \right) - P'_{ij}(y), \tag{30}$$

where

$$P_{qq}(z) = C_F \frac{1+z^2}{1-z} \quad (31)$$

$$P'_{qq}(z) = -C_F(1-z) \quad (32)$$

$$P_{gq}(z) = C_F \frac{1+(1-z)^2}{z} \quad (33)$$

$$P'_{gq}(z) = -C_F z \quad (34)$$

$$P_{gg}(z) = 2N \left[\frac{z}{1-z} + \frac{1-z}{z} + z(1-z) \right] \quad (35)$$

$$P'_{gg}(z) = 0 \quad (36)$$

$$P_{qg}(z) = \frac{1}{2} [z^2 + (1-z)^2] \quad (37)$$

$$P'_{qg}(z) = -z(1-z), \quad (38)$$

with $N = 3$.

3. Cross section in non-collinear region

As described above, the cross section in non-collinear region $d\sigma^{fin}$ can be easily obtained by Monte Carlo phase space integration in four dimension. It can be written as

$$\frac{d\sigma^{fin}}{dx_1 dx_2} = \sum_{q,q'} G_{q/A}(x_1, \mu_f) G_{q'/B}(x_2, \mu_f) |q q' \rightarrow t H^- X|^2 d\Phi_3 + [A \leftrightarrow B], \quad (39)$$

where q, q' run through gluon and light quarks and the three-body phase space Φ_3 is within the non-collinear region. In this paper, all Monte Carlo phase space integrations are performed by package BASES [13].

III. NUMERICAL RESULTS AND DISCUSSION

Our numerical results are obtained using CTEQ5M (CTEQ5L) PDF [14] and 2-loop (1-loop) evolution of $\alpha_s(\mu)$ for NLO (LO) cross section calculations with $\Lambda^{(5)} = 226$ (146) MeV. As we have mentioned in the second section, the dynamical mass of the bottom quark has been set to zero, which means that we treat the bottom quark as usual massless partons. For the process $bg \rightarrow t H^-$, this kind of choice is reasonable because the typical scale of the process is much higher than that of bottom quark. In our numerical calculations, 2-loop

evolution of the bottom and top quark mass is adopted in the \overline{MS} scheme. In the OS scheme, the top-quark mass is taken to be $m_t = 175$ GeV and the bottom quark mass is the same with that in the \overline{MS} scheme. For simplicity, the renormalization and factorization scales are taken to be the same.

A. Comparison between the results in the OS and \overline{MS} schemes

In Fig. 4, we show in (a): the LO and NLO cross sections in OS and \overline{MS} schemes and in (b): the relative deviation

$$\delta = \frac{\sigma_{OS} - \sigma_{\overline{MS}}}{\sigma_{OS} + \sigma_{\overline{MS}}} \quad (40)$$

as a function of renormalization and factorization scales μ/μ_0 ($\mu_0 = m_t + m_{H^\pm}$) for $m_{H^\pm} = 200$ GeV and $\tan\beta = 2$. From the figures we can see that

- scale-dependence in both schemes is smaller at NLO than that at LO
- the results in two schemes differ remarkably at tree-level (LO) and are significantly closer at the level including the QCD corrections (NLO).

For $\tan\beta = 2$, the contributions of bottom quark Yukawa coupling is much smaller than of top quark, we can write the cross section at LO in the two schemes as

$$\begin{aligned} \sigma_{LO}^{OS} &\propto m_t^2, \\ \sigma_{LO}^{\overline{MS}} &\propto \overline{m}_t(\mu)^2. \end{aligned} \quad (41)$$

Therefore

$$\delta_{LO} = \frac{m_t^2 - \overline{m}_t(\mu)^2}{m_t^2 + \overline{m}_t(\mu)^2} \simeq \frac{A}{2} \quad (42)$$

with (at one-loop order)

$$A = 2\frac{\alpha_s}{\pi} \left(\log \frac{\mu^2}{m_t^2} + \frac{4}{3} \right), \quad (43)$$

which is the quantity entering also the relation between the \overline{MS} quark mass and the corresponding pole mass,

$$m(\mu)^2 = m^2 [1 - A]. \quad (44)$$

For $\mu = 0.5\mu_0$ ($\mu_0, 2\mu_0$), $A \simeq 0.1(0.2, 0.3)$, therefore $\delta_{LO} \simeq 5\%(10\%, 15\%)$, as shown in Fig. 4 (b).

At NLO, we can write

$$\begin{aligned} \sigma_{NLO}^{OS} &\propto m_t^2 (1 - A + B), \\ \sigma_{NLO}^{\overline{MS}} &\propto \overline{m}_t(\mu)^2 (1 + B), \end{aligned} \quad (45)$$

where B is the $O(\alpha_s)$ radiative correction to the LO cross section in the \overline{MS} scheme. Hence, one finds

$$\delta_{NLO} \simeq \frac{AB}{2}. \quad (46)$$

For $\mu = 0.5\mu_0$ ($\mu_0, 2\mu_0$), we have $B \simeq 0.2(0.3, 0.4)$, and $\delta_{NLO} \simeq 1\%(3\%, 6\%)$.

From above discussion, we can conclude that the difference of the cross sections between the OS and \overline{MS} schemes at NLO: (1) is much smaller than that at LO; and (2) depends on two factors: the renormalization scale and the relative corrections in \overline{MS} scheme, and the latter is usually the order of $O(\alpha_s)$. Because the typical scale of the process is much higher than that of the b quark mass, it is appropriate to renormalize the b quark mass in the \overline{MS} scheme, in which the large term $\alpha_s \log(m_b^2/\mu^2)$ has been resummed into the running of the b quark mass. For the same reason, we will renormalize the top quark mass the same way and in next section give the numerical results in the \overline{MS} scheme.

B. Numerical results in the \overline{MS} scheme

In Fig. 5 we show the K-factor, which is defined as

$$K = \frac{\sigma_{NLO}}{\sigma_{LO}}, \quad (47)$$

as a function of the charged Higgs mass with the renormalization and factorization scales $\mu = \mu_0$. In the \overline{MS} scheme, the K-factor does not depend on $\tan\beta$, which is not true in the OS scheme because the different mass renormalization constants of top and bottom quark spoil it. The different contributions to K-factor from improved Born (which is equal

to 1 if the difference between the LO and NLO PDF and $\alpha_s(\mu)$ is omitted), virtual+gluon-radiation, initial-gluon, bq (\bar{q}) (q stand for the light quarks) and $q\bar{q}$ are also shown. From the figure, we can see that K-factor from improved Born contribution is around $1.2 \sim 1.3$. K-factor from virtual+gluon-radiation contribution is from 0.7 to 0.9 when the charged Higgs boson mass varies from 200 GeV to 1000 GeV. The initial-gluon and $bq(\bar{q})$ contributions to the K-factor are negative, and they vary from $\sim -27\%$ to $\sim -24\%$ and $\sim -5\%$ to $\sim -14\%$ respectively. The $q\bar{q}$ contribution to the K-factor can be neglected, the magnitude of which is smaller than 3% for all charged Higgs boson mass. Adding all the contributions, we can see that the K-factor varies from ~ 1.6 to ~ 1.8 when charged Higgs mass increases from 200 GeV to 1000 GeV.

It should be noted that if we replace the two-loop evolution quark mass by one-loop evolution one in the calculation of the LO cross section, in the \overline{MS} scheme,

$$K = f(Q) \frac{\overline{m}_{t,(2)}^2 + \overline{m}_{b,(2)}^2 \tan^4 \beta}{\overline{m}_{t,(1)}^2 + \overline{m}_{b,(1)}^2 \tan^4 \beta}, \quad (48)$$

where the subscript of quark mass is which kind of quark mass evolution is used, and $f(Q)$ is the function which is irrelevant to $\tan \beta$.

To summarize, the next-to-leading order QCD corrections to charged Higgs boson associated production with top quark through $bg \rightarrow tH^-$ at the CERN Large Hadron Collider are calculated in the minimal supersymmetric standard model and two-Higgs-doublet model in the \overline{MS} scheme. The NLO QCD corrections can reduce the scale dependence of the LO cross section. The K-factor varies from ~ 1.6 to ~ 1.8 when charged Higgs mass increases from 200 GeV to 1000 GeV. We should note here that the results presented in this paper are for the process $bg \rightarrow tH^-$; they are the same for the charge conjugate process $\bar{b}g \rightarrow H^+\bar{t}$.

IV. ACKNOWLEDGEMENT

The author would like to thank Prof. W. Hollik, Prof. C.S. Li, Prof. C.P. Yuan and Dr. J. Guasch for stimulating discussions. This work was supported in part by the Alexander von Humboldt Foundation and National Nature Science Foundation of China. Parts of the calculations have been performed on the QCM cluster at the University of Karlsruhe,

supported by the DFG-Forschergruppe ”Quantenfeldtheorie, Computeralgebra und Monte-Carlo-Simulation”.

[1] For example to see, L. G. Jin, C. S. Li, R. J. Oakes and S. H. Zhu, Phys. Rev. D **62**, 053008 (2000) [arXiv:hep-ph/0003159], and references therein.

[2] W. Hollik and S. h. Zhu, Phys. Rev. D **65**, 075015 (2002) [arXiv:hep-ph/0109103].

[3] D. P. Roy, Phys. Lett. B **459**, 607 (1999) [arXiv:hep-ph/9905542].

[4] K. Odagiri, Phys. Lett. B **452**, 327 (1999) [arXiv:hep-ph/9902303].

[5] F. Borzumati, J. L. Kneur and N. Polonsky, Phys. Rev. D **60**, 115011 (1999) [arXiv:hep-ph/9905443].

[6] L. G. Jin, C. S. Li, R. J. Oakes and S. H. Zhu, Eur. Phys. J. C **14**, 91 (2000) [arXiv:hep-ph/9907482].

[7] A. Belyaev, D. Garcia, J. Guasch and J. Sola, arXiv:hep-ph/0105053; C. S. Huang and S. H. Zhu, Phys. Rev. D **60**, 075012 (1999) [arXiv:hep-ph/9812201].

[8] G. p. Gao, G. r. Lu, Z. h. Xiong and J. M. Yang, arXiv:hep-ph/0202016.

[9] J. Küblbeck, M. Böhm and A. Denner, Comput. Phys. Commun. **60**, 165 (1990); T. Hahn, hep-ph/9905354.

[10] R. Mertig, M. Böhm and A. Denner, Comput. Phys. Commun. **64**, 345 (1991).

[11] W. Beenakker, R. Hopker, M. Spira and P. M. Zerwas, Nucl. Phys. B **492**, 51 (1997) [arXiv:hep-ph/9610490].

[12] For example to see, B. W. Harris and J. F. Owens, hep-ph/0102128; S. h Zhu, Phys. Lett. B **524**, 283 (2002), hep-ph/0109269.

[13] S. Kawabata, Comput. Phys. Commun. 88, 309 (1995).

[14] H. L. Lai *et al.* [CTEQ Collaboration], Eur. Phys. J. C **12**, 375 (2000) [hep-ph/9903282].

[15] G. J. van Oldenborgh and J. A. Vermaseren, Z. Phys. C **46**, 425 (1990).

V. APPENDIX

In this appendix, we will give the non-vanishing form-factors in Eq. (16). For completeness, we give firstly the definition of loop integrals and its Lorentz decomposition:

$$B_0(p_1^2, m_0^2, m_1^2) = \frac{(2\pi\mu)^{4-d}}{i\pi^2} \int d^d q \frac{1}{Q_0 Q_1}, \quad (49)$$

$$C_{0;\mu;\mu\nu}(p_1^2, p_{12}, p_2^2, m_0^2, m_1^2, m_2^2) = \frac{(2\pi\mu)^{4-d}}{i\pi^2} \int d^d q \frac{1; q_\mu; q_\mu q_\nu}{Q_0 Q_1 Q_2}, \quad (50)$$

$$D_{0;\mu;\mu\nu}(p_1^2, p_{12}, p_{32}, p_3^2, p_2^2, p_{31}, m_0^2, m_1^2, m_2^2, m_3^2) = \frac{(2\pi\mu)^{4-d}}{i\pi^2} \int d^d q \frac{1; q_\mu; q_\mu q_\nu}{Q_0 Q_1 Q_2 Q_3} \quad (51)$$

with

$$Q_0 = q^2 - m_0^2 + i\epsilon, \quad Q_i = (q + p_i)^2 - m_i^2 + i\epsilon, \quad p_{ij} = (p_i - p_j)^2 \quad (52)$$

and

$$\begin{aligned} C_\mu &= p_{1\mu} C_1 + p_{2\mu} C_2 \\ C_{\mu\nu} &= g_{\mu\nu} C_{00} + p_{1\mu} p_{1\nu} C_{11} + (p_{1\mu} p_{2\nu} + p_{2\mu} p_{1\nu}) C_{12} + p_{2\mu} p_{2\nu} C_{22} \\ D_\mu &= p_{1\mu} D_1 + p_{2\mu} D_2 + p_{3\mu} D_3 \\ D_{\mu\nu} &= g_{\mu\nu} D_{00} + p_{1\mu} p_{1\nu} D_{11} + (p_{1\mu} p_{2\nu} + p_{2\mu} p_{1\nu}) D_{12} + (p_{1\mu} p_{3\nu} + p_{3\mu} p_{1\nu}) D_{13} \\ &\quad + p_{2\mu} p_{2\nu} D_{22} + (p_{2\mu} p_{3\nu} + p_{3\mu} p_{2\nu}) D_{23} + p_{3\mu} p_{3\nu} D_{33}. \end{aligned} \quad (53)$$

For simplicity, we define abbreviation for $B_0^i (i = 1 - 7)$, $C_x^i (i = 1 - 8)$ [x stands for the subscript defined in Eq. (53)], $D_0^i (i = 1 - 3)$ as

$$\begin{aligned} B_0^1 &= B_0(0, 0, m_t^2), \\ B_0^2 &= B_0(0, m_t^2, m_t^2), \\ B_0^3 &= B_0(m_{H^\pm}^2, 0, m_t^2), \\ B_0^4 &= B_0(m_t^2, 0, m_t^2), \end{aligned}$$

$$\begin{aligned}
B_0^5 &= B_0(s, 0, 0), \\
B_0^6 &= B_0(t, 0, m_t^2), \\
B_0^7 &= B_0(u, 0, m_t^2), \\
C_x^1 &= C_x(0, 0, s, 0, 0, 0), \\
C_x^2 &= C_x(0, m_{H^\pm}^2, t, m_t^2, m_t^2, 0), \\
C_x^3 &= C_x(m_{H^\pm}^2, 0, t, m_t^2, 0, 0), \\
C_x^4 &= C_x(m_{H^\pm}^2, 0, u, m_t^2, 0, 0), \\
C_x^5 &= C_x(m_{H^\pm}^2, m_t^2, s, 0, m_t^2, 0), \\
C_x^6 &= C_x(m_t^2, 0, t, m_t^2, 0, 0), \\
C_x^7 &= C_x(m_t^2, 0, u, 0, m_t^2, m_t^2), \\
C_x^8 &= C_x(m_t^2, 0, u, m_t^2, 0, 0), \\
D_0^1 &= D_0(m_{H^\pm}^2, 0, m_t^2, 0, t, u, 0, m_t^2, m_t^2, 0), \\
D_0^2 &= D_0(m_{H^\pm}^2, m_t^2, 0, 0, s, t, 0, m_t^2, 0, 0), \\
D_0^3 &= D_0(m_{H^\pm}^2, m_t^2, 0, 0, s, u, 0, m_t^2, 0, 0).
\end{aligned} \tag{54}$$

For diagram (e) in Fig. 2, we can write the form factor as

$$f_i = \frac{C_A}{2} \frac{g_s^3}{16\pi^2 s} g_i \tag{55}$$

$$\begin{aligned}
g_2 &= -2B_0^5 - s[C_0^1 + 3(C_1^1 + C_2^1)] + 4(-1 + 2\epsilon)C_{00}^1, \\
g_5 &= 2[B_0^5(1 + \epsilon) + s(C_0^1 + 2C_1^1 - 3C_2^1)].
\end{aligned} \tag{56}$$

For diagram (f) in Fig. 2, we can write the form factor as

$$f_i = (C_F - C_A/2) \frac{g_s^3}{8\pi^2 s} g_i \tag{57}$$

$$\begin{aligned}
g_2 &= -B_0^5 - (1 + \epsilon)s(C_0^1 + C_1^1 + C_2^1) + 2(1 - \epsilon)C_{00}^1, \\
g_5 &= (1 + \epsilon)B_0^5 + 2\epsilon s C_1^1 - 2(1 + \epsilon)s C_2^1.
\end{aligned} \tag{58}$$

For diagram (g) in Fig. 2, we can write the form factor as

$$f_i = C_F \frac{g_s^3}{8\pi^2 s} g_i \tag{59}$$

$$\begin{aligned} g_1 &= m_t s (C_0^5 (1 - \epsilon) + C_2^5 - \epsilon (C_1^5 + C_2^5)), \\ g_2 &= \frac{g_5}{2} = C_0^5 (m_{H^\pm}^2 - 2m_t^2) - B_0^4 - B_0^5 - m_t^2 (C_1^5 + C_2^5) + \epsilon (B_0^3 + s C_2^5). \end{aligned} \quad (60)$$

For diagram (h) in Fig. 2, we can write the form factor as

$$f_i = C_F \frac{g_s^3}{8\pi^2(m_t^2 - u)} g_i \quad (61)$$

$$\begin{aligned} g_1 &= m_t (-1 + \epsilon) (m_t^2 - u) (C_0^4 + C_1^4 + C_2^4), \\ g_2 &= \frac{g_3}{2} = -C_0^4 [m_{H^\pm}^2 + (-2 + \epsilon) m_t^2 - \epsilon u] + B_0^7 \\ &\quad + m_t^2 (C_1^4 + C_2^4) - \epsilon [B_0^3 + (m_t^2 - u) (C_1^4 + C_2^4)]. \end{aligned} \quad (62)$$

For diagram (i) in Fig. 2, we can write the form factor as

$$f_i = \frac{C_A}{2} \frac{g_s^3}{16\pi^2(m_t^2 - u)} g_i \quad (63)$$

$$\begin{aligned} g_1 &= 3m_t (m_t^2 - u) C_2^8, \\ g_2 &= 2B_0^4 + 2B_0^7 + (m_t^2 - u) (2C_0^8 + 3C_1^8) + 4(1 - \epsilon) C_{00}^8, \\ g_3 &= 2\{\epsilon - 1 + C_0^8 (m_t^2 - u) - (1 + \epsilon) B_0^4 + 2B_0^7 + m_t^2 [-5C_1^8 + 4C_2^8 + 2(1 - \epsilon) C_{11}^8] \\ &\quad + u [C_1^8 - 4C_2^8 - 2(1 - \epsilon) C_{11}^8]\}, \\ g_4 &= 4m_t [C_1^8 - 2C_2^8 - (1 - \epsilon) C_{11}^8]. \end{aligned} \quad (64)$$

For diagram (j) in Fig. 2, we can write the form factor as

$$f_i = (C_F - C_A/2) \frac{g_s^3}{8\pi^2(m_t^2 - u)} g_i \quad (65)$$

$$\begin{aligned} g_1 &= m_t (m_t^2 - u) [C_2^7 + \epsilon (C_0^7 + C_2^7)], \\ g_2 &= 2C_0^7 m_t^2 - (1 + \epsilon) B_0^2 + B_0^4 + B_0^7 + (1 + \epsilon) (m_t^2 - u) C_1^7 + 2(-1 + \epsilon) C_{00}^7, \\ g_3 &= -1 - B_0^4 + 2B_0^7 + 2u C_{22}^7 - 2m_t^2 (2C_2^7 + C_{22}^7) \\ &\quad - \epsilon [-1 + B_0^4 - 2(m_t^2 - u) (C_2^7 + C_{22}^7)], \\ g_4 &= -2m_t [C_0^7 \epsilon + (-1 + 2\epsilon) C_2^7 + (-1 + \epsilon) C_{22}^7]. \end{aligned} \quad (66)$$

For diagram (k) in Fig. 2, we can write the form factor as

$$f_i = C_F \frac{g_s^3}{16\pi^2 s} g_i \quad (67)$$

$$g_2 = \frac{g_5}{2} = (1 - \epsilon) B_0^5. \quad (68)$$

For diagram (l) in Fig. 2, we can write the form factor as

$$f_i = C_F \frac{g_s^3}{16\pi^2 (m_t^2 - u)^2 u} g_i \quad (69)$$

$$\begin{aligned} g_1 &= -m_t(m_t^2 - u) \left\{ (\epsilon - 1)m_t^2(B_0^1 - B_0^7) + u(\epsilon - 3)B_0^7 \right\}, \\ g_2 &= \frac{g_3}{2} = (-1 + \epsilon)m_t^4(B_0^1 - B_0^7) - (-1 + \epsilon)u^2 B_0^7 \\ &\quad + m_t^2 u \left\{ (1 - \epsilon)[B_0^1 - 2(1 + B_0^2)] \right\} + 2(-3 + \epsilon)B_0^7. \end{aligned} \quad (70)$$

For diagram (m) in Fig. 2, we can write the form factor as

$$f_i = \frac{C_A}{2} \frac{g_s^3}{16\pi^2} g_i \quad (71)$$

$$\begin{aligned} g_1 &= -m_t[C_0^8 + C_1^8 + C_2^8 - 2(s - u + m_t^2)(D_0^3 + D_1 + D_2 + D_3) + 4D_{00}], \\ g_2 &= -2(C_0^4 + C_0^5) - 2D_0^3(m_t^2 - u) + C_1^1 + C_1^8 + 2(t + 2u)(D_2 + D_3) \\ &\quad - m_{H^\pm}^2(D_1 + 2D_2 + D_3) - m_t^2(D_1 + 4D_2 + 3D_3) + 4\epsilon D_{00}, \\ g_3 &= -2 \left\{ 2[C_0^4 - (1 + \epsilon)C_0^5 + C_0^8] - 2\epsilon(C_1^5 + C_2^5) + C_1^8 + C_2^8 + 2D_0^3[-m_{H^\pm}^2 + (1 - \epsilon)m_t^2 \right. \\ &\quad \left. + (1 + \epsilon)u] + 2[(3 - 2\epsilon)m_t^2 - t + 2u\epsilon](D_1 + D_2 + D_3) + 2[(1 - \epsilon)m_t^2 + u\epsilon](D_{11} \right. \\ &\quad \left. + 2D_{12} + 2D_{13} + D_{22} + 2D_{23} + D_{33}) \right\}, \\ g_4 &= 4m_t \left\{ (D_2 + D_3 + D_{11} + 2D_{12} + D_{13} + D_{22} + D_{23}) - \epsilon[D_0^3 + D_{11} + D_{22} + D_{33} \right. \\ &\quad \left. + 2(D_1 + D_2 + D_3 + D_{12} + D_{13} + D_{23})] \right\}, \\ g_5 &= 4m_t \left\{ C_0^1 + 2\epsilon C_1^5 - C_1^1 + 2(u - m_t^2)D_1 + [m_{H^\pm}^2 - (7 - 2\epsilon)m_t^2 + 2(t + 2u) - 2u\epsilon]D_2 \right. \\ &\quad \left. + [-m_{H^\pm}^2 - m_t^2 + 2s]D_3 + [2(\epsilon - 1)m_t^2 - 2u\epsilon](D_{12} + D_{22} + D_{23}) \right\}, \\ g_6 &= -4m_t[D_0^3 + D_1 + (2 - \epsilon)D_2 + D_3 + D_{12} + D_{22}], \end{aligned} \quad (72)$$

where the variable of the D-function is the same with D_0^3 .

For diagram (n) in Fig. 2, we can write the form factor as

$$f_i = (C_F - C_A/2) \frac{g_s^3}{8\pi^2} g_i \quad (73)$$

$$\begin{aligned}
g_1 &= -m_t \left\{ D_0^1[s + \epsilon(m_t^2 - u)] + s(D_2 + D_3) \right. \\
&\quad \left. - \epsilon[C_2^6 - m_t^2(D_1 + D_3) + u(D_2 + D_3)] - 2D_{00} \right\}, \\
g_2 &= -C_0^4 - C_0^7 + C_0^2(2 + \epsilon) + D_0^1[m_{H^\pm}^2 + \epsilon m_t^2 - (2 + \epsilon)u] + D_1[m_t^2(1 + \epsilon) \\
&\quad + s - u(1 + \epsilon)] + (D_2 + D_3)[\epsilon m_t^2 + s - u(1 + \epsilon)] - 2\epsilon D_{00}, \\
g_3 &= 2 \left\{ -C_0^4 - C_0^7 - (C_1^7 + C_2^7) - \epsilon(C_1^2 + C_2^6) + 2m_t^2 D_2 - t(D_2 + D_3) + m_t^2(2D_3 + D_{22} \right. \\
&\quad \left. + 2D_{23} + D_{33}) - \epsilon \left[C_2 + (m_t^2 - u)[D_2 + D_3 + D_{22} + 2D_{23} + D_{33}] \right] \right\}, \\
g_4 &= 2m_t \left\{ -D_2 - D_3 - D_{12} - D_{13} - D_{22} - 2D_{23} - D_{33} \right. \\
&\quad \left. + \epsilon[D_0^1 + 2D_2 + 2D_3 + D_{22} + 2D_{23} + D_{33}] \right\}, \\
g_5 &= -2 \left\{ C_0^6(-1 + \epsilon) + (4m_t^2 - t - 2u)D_2 - sD_3 + m_t^2(D_{22} + D_{23}) \right. \\
&\quad \left. + \epsilon[2C_1^6 - C_1^2 + C_2^6 - (m_t^2 - u)(D_3 + D_{22} + D_{23})] \right\}, \\
g_6 &= 2m_t[D_0 - (-3 + \epsilon)D_2 + D_{12} - (-1 + \epsilon)(D_{22} + D_{23})], \tag{74}
\end{aligned}$$

where the variable of the D-function is the same with D_0^1 .

For diagram (o) in Fig. 2, we can write the form factor as

$$f_i = (C_F - C_A/2) \frac{g_s^3}{8\pi^2} g_i \tag{75}$$

$$\begin{aligned}
g_1 &= -m_t[C_0^5 - \epsilon C_0^6 + D_0^2(1 + \epsilon)s - \epsilon(C_1^6 + C_2^6) + s(1 + \epsilon)(D_1 + D_2 + D_3) - 2D_{00}], \\
g_2 &= -C_0^1 - C_0^5 + C_0^3(2 + \epsilon) + D_0^2(-2m_t^2 + t) - m_t^2(D_1 + D_2) \\
&\quad + [s(1 + \epsilon) - u]D_3 - 2\epsilon D_{00}, \\
g_3 &= 2 \left\{ C_0^5(1 + \epsilon) - C_0^6\epsilon + D_0^2[2m_{H^\pm}^2 + m_t^2(4 - \epsilon) - s(2 - \epsilon) - 3t - u(2 - \epsilon)] \right. \\
&\quad \left. + \epsilon(C_1^3 + C_1^5 - C_1^6 + C_2^5 - C_2^6) + (D_1 + D_2 + D_3)[m_{H^\pm}^2(-3 + \epsilon) - m_t^2\epsilon + 3s + t(2 - \epsilon) \right. \\
&\quad \left. + u(3 + \epsilon)] + (D_{11} + 2D_{12} + 2D_{13} + D_{22} + 2D_{23} + D_{33})[m_t^2(1 - \epsilon) + \epsilon u] \right\}, \\
g_4 &= 2m_t \left\{ -D_3 - D_{13} - D_{23} - D_{33} + \epsilon(D_0 + 2D_1 + 2D_2 + 2D_3 + D_{11} \right. \\
&\quad \left. + 2D_{12} + 2D_{13} + D_{22} + 2D_{23} + D_{33}) \right\}, \\
g_5 &= -2 \left\{ C_0^6 - D_0^2(m_{H^\pm}^2 - 2m_t^2) - C_1^1 + \epsilon(C_1^3 + C_2^5) + D_1[-t(1 + \epsilon) - 2u] + \right. \\
&\quad (D_2 + D_3)[\epsilon m_{H^\pm}^2 - s(1 + \epsilon)] + D_3[-t(1 + \epsilon) - u] + (D_{11} + D_{12} + 2D_{13} + D_{23} + D_{33})u\epsilon \\
&\quad \left. + m_t^2[5D_1 + D_2 + 4D_3 - (-1 + \epsilon)(D_{11} + D_{12} + 2D_{13} + D_{23} + D_{33})] \right\}, \\
g_6 &= 2m_t \left\{ D_0^2 - (-2 + \epsilon)(D_1 + D_3) + D_{13} + D_{33} - \epsilon(D_{11} + D_{12} + 2D_{13} + D_{23} + D_{33}) \right\}, \tag{76}
\end{aligned}$$

where the variable of the D-function is the same with D_0^2 .

By decomposition, the loop integrals in above form-factors can be calculated by the limit number of scalar integrals B_0, C_0 and D_0 . The scalar integrals C_0 and D_0 are UV finite, however some of them contain infrared and collinear divergences. Because the finite scalar integrals could be calculated by numerical method [15], only the divergent ones are presented explicitly in this paper. It should be noted that only real part of the integrals, which is relevant to our results, is given.

D_0 and C_0 scalar integrals could be generally written as

$$\begin{aligned} D_0 &= (4\pi\mu^2)^\epsilon \Gamma(1+\epsilon) \left(\frac{d_2}{\epsilon^2} + \frac{d_1}{\epsilon} + d_0 \right), \\ C_0 &= -(4\pi\mu^2)^\epsilon \Gamma(1+\epsilon) \left(\frac{c_2}{\epsilon^2} + \frac{c_1}{\epsilon} + c_0 \right). \end{aligned} \quad (77)$$

The coefficients d_2, d_1 and d_0 of D_0^1 are

$$d_2 = \frac{1}{2 (m_t^2 - t) (m_t^2 - u)}, \quad (78)$$

$$d_1 = \frac{1}{(m_t^2 - t) (m_t^2 - u)} \log \frac{m_t (m_t^2 - m_{H^\pm}^2)}{(m_t^2 - t) (m_t^2 - u)}, \quad (79)$$

$$\begin{aligned} d_0 = & \frac{1}{2 (m_t^2 - t) (m_t^2 - u)} \left\{ \pi^2 \left[\theta(m_{H^\pm} - m_t) - \frac{1}{3} \right] - 2 \log^2 m_t + 3 \log^2(m_t^2 - t) \right. \\ & + 3 \log^2(m_t^2 - u) - 2 \log(m_t^2 - t) \log(t) - 2 \log(m_t^2 - u) \log(u) - 3 \log^2 |m_{H^\pm}^2 - m_t^2| \\ & + 4 \log(m_{H^\pm}) \log \frac{m_{H^\pm}^2 - m_t^2}{m_t^2} - 4 \log(m_t) \log \frac{(m_t^2 - t)(m_t^2 - u)}{tu(m_{H^\pm}^2 - m_t^2)} - 2li_2 \left(\frac{m_{H^\pm}^2 s}{(m_{H^\pm}^2 - t)(m_{H^\pm}^2 - u)} \right) \\ & - 2li_2 \left(\frac{(m_t^2 - t)u}{m_t^2(u - m_{H^\pm}^2)} \right) - 2li_2 \left(\frac{m_t^2}{m_t^2 - m_{H^\pm}^2} \right) + 2li_2 \left(\frac{u - m_{H^\pm}^2}{m_t^2 - t} \right) + 2li_2 \left(\frac{m_t^2}{m_t^2 - t} \right) \\ & + 2li_2 \left(\frac{t - m_{H^\pm}^2}{m_t^2 - u} \right) - 2li_2 \left(\frac{(t - m_{H^\pm}^2)(u - m_{H^\pm}^2)}{(m_t^2 - t)(m_t^2 - u)} \right) + 2li_2 \left(\frac{m_t^2}{m_t^2 - u} \right) - 2li_2 \left(\frac{t(u - m_t^2)}{m_t^2(m_{H^\pm}^2 - t)} \right) \\ & + 2li_2 \left(\frac{m_{H^\pm}^2 (m_t^2 - t)(m_t^2 - u)}{m_t^2(m_{H^\pm}^2 - u)(m_{H^\pm}^2 - t)} \right) + 2li_2 \left(\frac{ts}{(m_{H^\pm}^2 - t)(t - m_t^2)} \right) \\ & \left. - 2li_2 \left(\frac{m_t^2 s}{(m_t^2 - t)(m_t^2 - u)} \right) + 2li_2 \left(\frac{su}{(m_{H^\pm}^2 - u)(u - m_t^2)} \right) \right\}. \end{aligned} \quad (80)$$

The coefficients d_2, d_1 and d_0 of D_0^2 are

$$d_2 = \frac{3}{2 s (t - m_t^2)}, \quad (81)$$

$$d_1 = \frac{1}{s(t - m_t^2)} \log \frac{m_t(m_{H^\pm}^2 - m_t^2)}{s(m_t^2 - t)^2}, \quad (82)$$

$$d_0 = \frac{1}{2s(m_t^2 - t)} \left\{ \pi^2 [1 - \theta(m_{H^\pm} - m_t)] + 2\log^2(m_t) + \log^2|m_{H^\pm}^2 - m_t^2| - \log^2(m_t^2 - t) \right. \\ \left. - 2\log(m_{H^\pm}^2 - t)\log(m_t^2 - t) + 4\log \frac{s}{m_{H^\pm}^2 - t} \log \frac{m_t}{m_t^2 - t} - 2li_2\left(\frac{m_{H^\pm}^2}{m_{H^\pm}^2 - m_t^2}\right) \right. \\ \left. + 2li_2\left(\frac{m_t^2 - t}{m_t^2}\right) - 2li_2\left(\frac{m_{H^\pm}^2(m_t^2 - t)}{m_t^2(m_{H^\pm}^2 - t)}\right) + 2li_2\left(\frac{m_{H^\pm}^2}{m_t^2 - t}\right) + 2li_2\left(\frac{m_{H^\pm}^2 - t}{m_t^2 - t}\right) \right\}. \quad (83)$$

The coefficients c_2, c_1 and c_0 of C_0^1 are

$$c_2 = -\frac{1}{s}, \quad (84)$$

$$c_1 = \frac{\log(s)}{s}, \quad (85)$$

$$c_0 = \frac{1}{6s} [4\pi^2 - 3\log^2(s)]. \quad (86)$$

The coefficients c_1 and c_0 of C_0^3 are

$$c_1 = \frac{1}{m_{H^\pm}^2 - t} \log \left(\frac{m_t^2 - m_{H^\pm}^2}{m_t^2 - t} \right), \quad (87)$$

$$c_0 = \frac{1}{2(m_{H^\pm}^2 - t)} \left\{ \log^2(m_t^2 - t) - \log^2(m_t^2 - m_{H^\pm}^2) + 2li_2\left(\frac{m_{H^\pm}^2}{m_{H^\pm}^2 - m_t^2}\right) - 2li_2\left(\frac{t}{t - m_t^2}\right) \right\}. \quad (88)$$

The coefficients c_2, c_1 and c_0 of C_0^6 are

$$c_2 = \frac{1}{2(m_t^2 - t)}, \quad (89)$$

$$c_1 = \frac{1}{(m_t^2 - t)} \log \frac{m_t}{m_t^2 - t}, \quad (90)$$

$$c_0 = \frac{1}{2(m_t^2 - t)} \left\{ -\log(m_t) + \log^2(m_t^2 - t) - 2li_2\left(\frac{t}{t - m_t^2}\right) \right\}. \quad (91)$$

C_0^4, C_0^8 and D_0^3 can be obtained from C_0^3, C_0^6 and D_0^2 by replacing t with u .

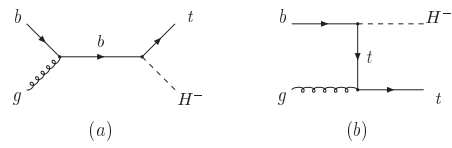


FIG. 1. Feynman diagrams at LO for $bg \rightarrow tH^-$.

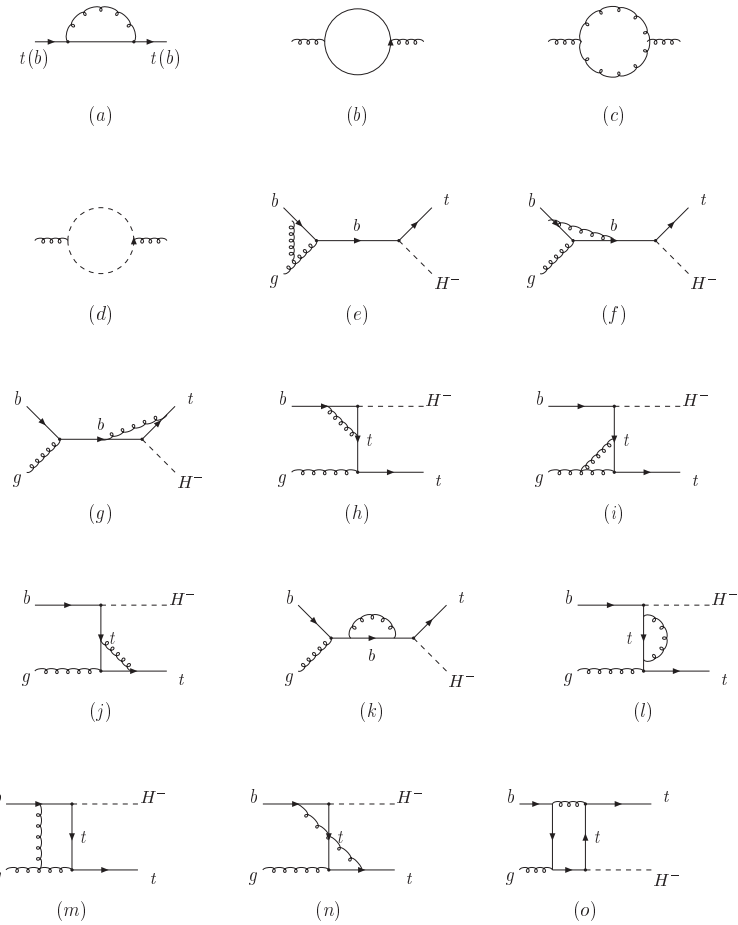


FIG. 2. Feynman diagrams of the virtual correction for the process $bg \rightarrow tH^-$.

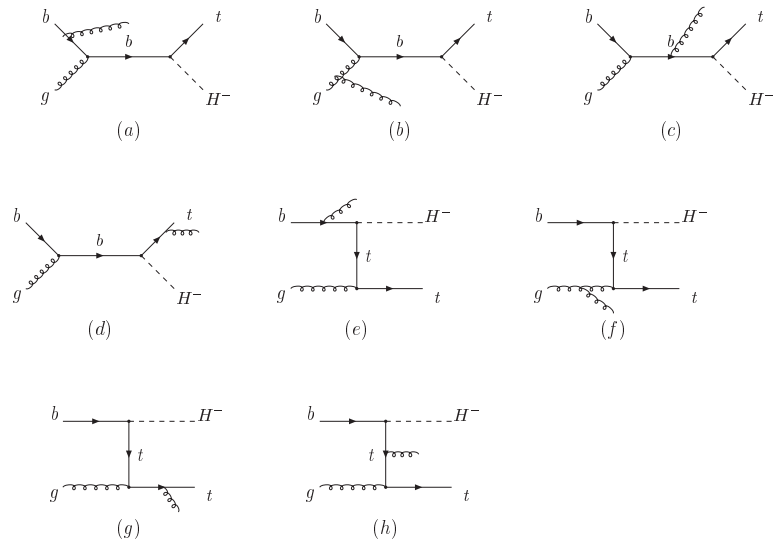


FIG. 3. Feynman diagrams of gluon-radiation process of $bg \rightarrow tH^- g$.

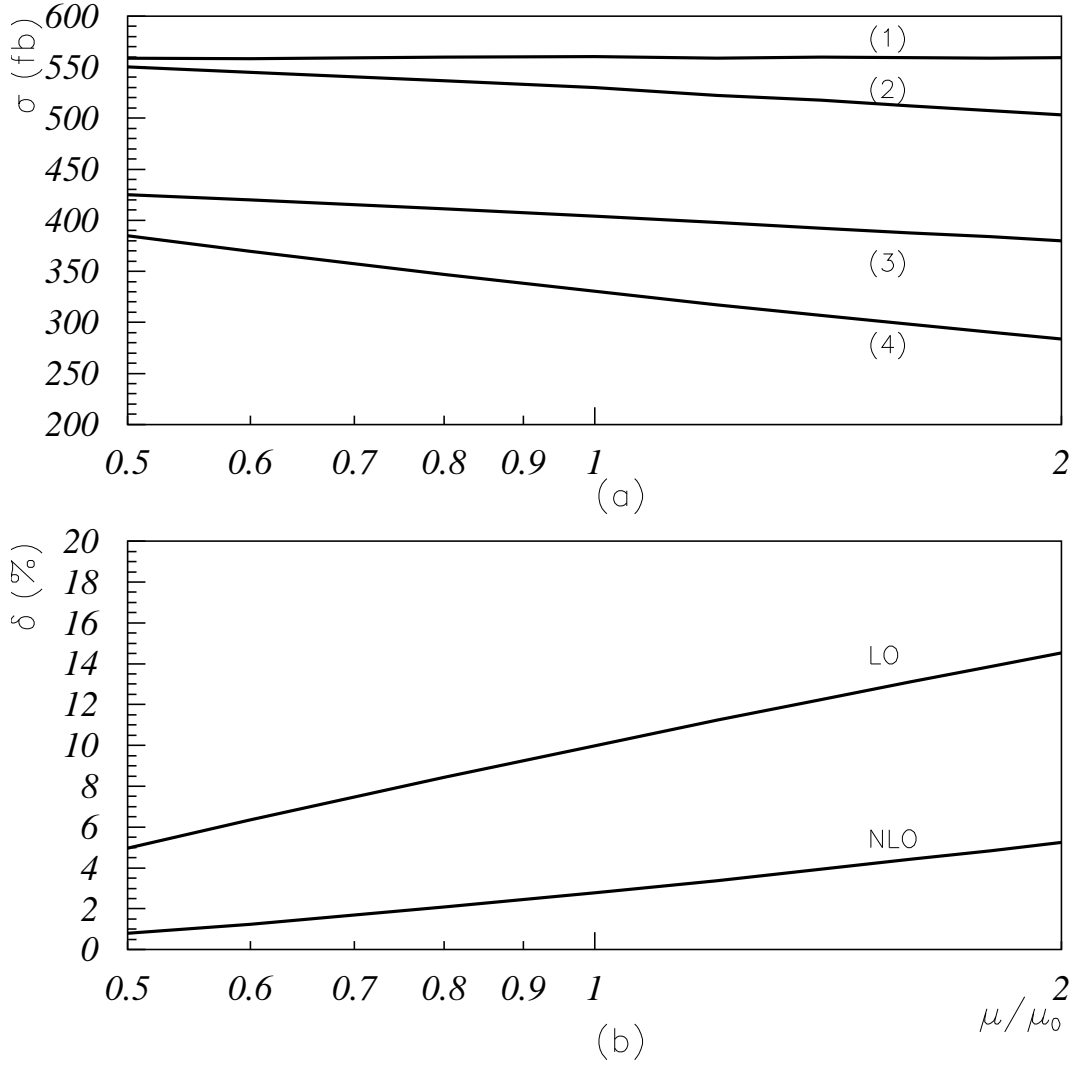


FIG. 4. (a): the total cross sections as a function of μ/μ_0 with $\mu_0 = m_{H^\pm} + m_t$, where $\tan \beta = 2$ and $m_{H^\pm} = 200$ GeV. Curves (1)-(4) represent the cross section at NLO in OS scheme (1), NLO in \overline{MS} scheme (2), LO in OS scheme (3), LO in \overline{MS} scheme (4). (b): δ (defined in text) as a function of μ/μ_0 .

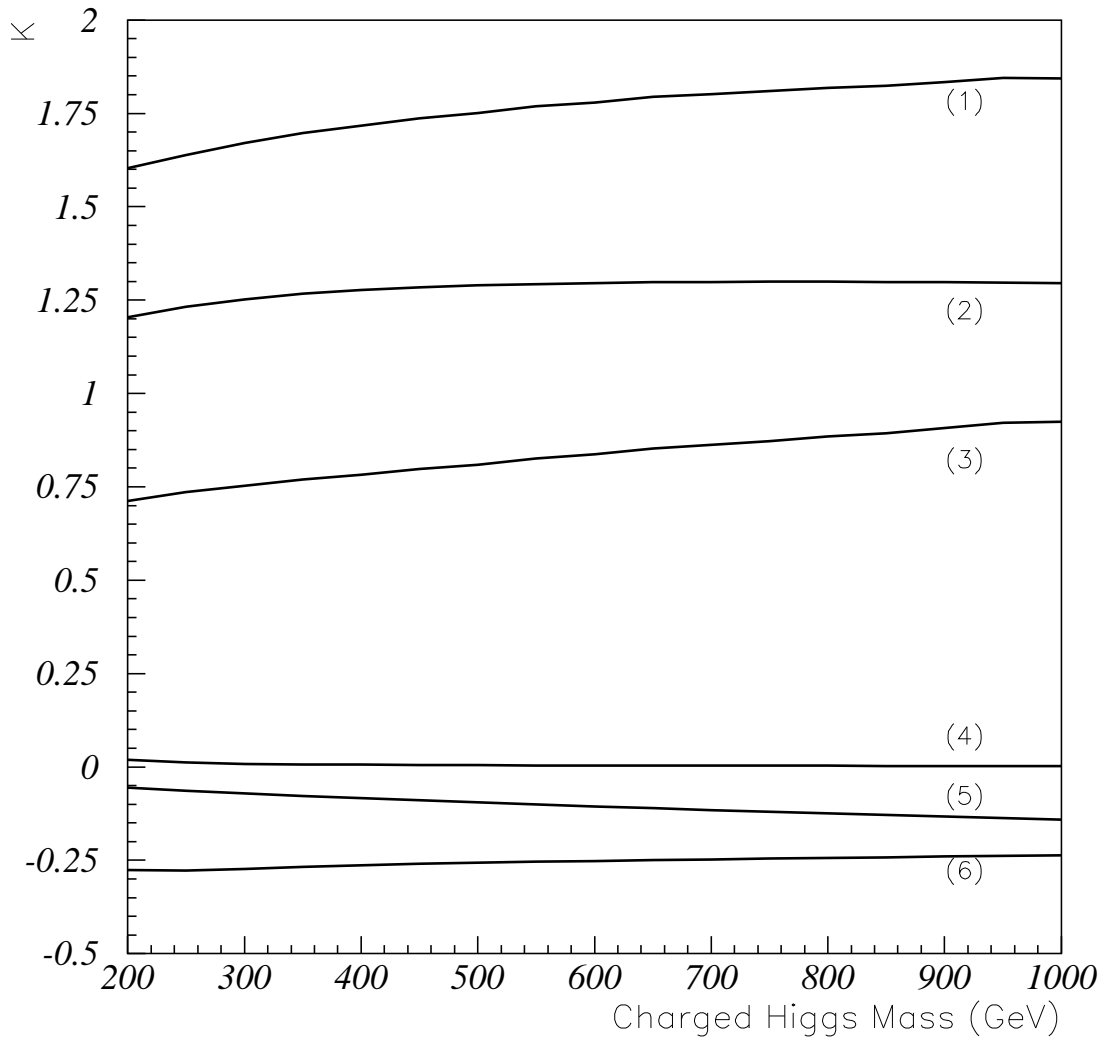


FIG. 5. Various contributions to K-factor versus m_{H^\pm} . Curves (1)-(6) represent contributions from all (1), improved Born (2), virtual plus gluon-radiation (3), $q\bar{q}$ (4), $bq(\bar{q})$ (5) and initial-gluon (6).